Korean J. Chem. Eng., **30**(3), 518-527 (2013)
DOI: 10.1007/s11814-012-0163-4

Simulation and analysis of dehydration distillation column based on distillation mechanism integrated with neural network

Qingtao Sun‡, Chunjian Pan‡, and Xuefeng Yan†

Key Laboratory of Advanced Control and Optimization for Chemical Processes of Ministry of Education, East China University of Science and Technology, Shanghai 200237, P. R. China
(*Received 3 November 2011 • accepted 22 September 2012*)

Abstract−In an industrial solvent dehydration distillation column (SDDC) model, the Murphree efficiency represents the separation ability of a distillation tray and the SDDC model's performance depends on the value accuracy of the Murphree efficiency. Because there are many operation conditions having nonlinear effect on Murphree efficiency, it is difficult to determine its value. To develop a precise and robust SDDC model, a novel hybrid model combining distillation mechanism with neural network is proposed. In the SDDC hybrid model, the neural network is employed to model the nonlinear relationship between the operation conditions and Murphree efficiency, which is embedded into the SDDC mechanistic model. The results showed a good predicting and robust performance of the hybrid model under different operation conditions. Based on the hybrid model, the effect of the operation conditions on SDDC was analyzed to obtain some useful guiding rules for the SDDC operation.

Key words: Hybrid Model, Murphree Efficiency, Neural Networks, Dehydratic Distillation

INTRODUCTION

In the production of terephthalic acid (TA), the well-known industrial process for the liquid-phase catalytic oxidation of p-xylene (PX) to TA by air or molecular oxygen in the temperature range of 150-210 °C in an industrial type of continuous stirred tank reactor (CSTR) is widely adopted. In the industrial oxidation process, cobalt and manganese acetates (Co(Ac)2 and Mn(Ac)2) are employed as catalysts, hydrogen bromide (HBr) acts as catalyst promoter reducing the induction period, and acetic acid (HAc) is used as reaction solvent. During the oxidation process, the water, which has an effect on the oxidation reaction (i.e., prevents the oxidation reaction), is produced. To remove the water, the solvent is sent to a solvent dehydration distillation column (SDDC) and then the fresh dehydration solvent is recycled to the CSTR [1,2]. The solvent dehydration is an important unit in the production of TA because the water concentration of the feed into the CSTR depends on the water concentration of the fresh dehydration solvent outlet from the SDDC.

Because using conventional distillation to separate HAc and water would require more equilibrium stages and a large reflux ratio, n-propyl-Acetate (NPA) is employed as an entrainer in an industrial SDDC. Namely, it is a heterogeneous azeotropic distillation column for the separation of HAc and water. The design of an HAc dehydration distillation system with an entrainer has been studied in several publications. Othmer [3] described an azeotropic distillation system containing a dehydrating column, a decanter, and a distillation column for the separation of HAc and H_2O. Chien et al. [4] studied the design and control of the HAc dehydration system via heterogeneous azeotropic distillation. Some other investigations such as parametric sensitivity, multiple steady states, long transient and nonlinear dynamics on the HAc azeotropic dehydration distillation were comprehensively reviewed by Widagdo and Seider [5]. The references primarily focus on the mechanism, design and control of HAc dehydration distillation system, develop the models with constant efficiencies of distillation trays based on a steady operation condition, and seldom consider the effect of the operation condition of column on the efficiencies of distillation trays. Considering that the operation conditions of industrial SDDC have a high nonlinear effect on the separation efficiencies of distillation trays and are often adjusted according to the practical production, the developed models are unfit for predicting the behavior of the industrial SDDC when the operation conditions are far from the specific steady operation conditions used for modeling.

To develop an accurate and robust model of the industrial SDDC, a novel hybrid model of SDDC, which combines distillation mechanism with artificial neural network, is proposed. In this hybrid model, an artificial neural network (ANN) is employed to develop the model of the tray efficiency influenced by the operation conditions, and then it is embedded into the distillation mechanism model. Thus, according to the different operation conditions of the industrial SDDC, the corresponding tray efficiency can be obtained via the ANN model of the tray efficiency. And then, based on the obtained tray efficiency, the distillation mechanism in the hybrid model is used to predict the behavior of the industrial SDDC. In the practical application of the industrial SDDC, the results demonstrate the merits of the hybrid model: good accuracy and robustness.

The remaining of this article is organized as follows. Section 2 introduces the feed-forward neural network. Section 3 briefly introduces the distillation mechanism of SDDC. In section 4, to model the tray efficiency, the sample data is constructed and a feed-forward neural network is employed. In section 5, the procedure of the hybrid model combining the distillation mechanism with the ANN model

†To whom correspondence should be addressed.
E-mail: xfyan@ecust.edu.cn
‡These authors contributed equally to this work.

of the tray efficiency is presented, the performance of the hybrid model for the practical industrial SDDC is demonstrated, and some guiding rules are obtained based on the hybrid model. Finally, a conclusion is presented in Section 6.

FEED-FORWARD BP NEURAL NETWORKS

Feed-forward neural network is the most common artificial neural network structure [6-9]. With as few as one hidden layer and sufficient hidden neurons, the feed-forward neural network can approximate very well almost any function in applications [10]. Thus, in our work, the feed-forward neural network with the three layers, input layer, hidden layer and output layer, was employed. The numbers of input and output neurons equal to the numbers of the input and output elements. When the number of the hidden neurons is determined, the structure of the feed-forward neural network is determined. Based on a training sample, back propagation algorithm (BP) is one of the most popular algorithms for training a network [11-13].

DISTILLATION MECHANISM MODEL FOR SDDC

1. Flow Chart of Industrial SDDC

Fig. 1 shows the flow chart of an industrial SDDC. In the industrial SDDC, a dehydration distillation column (denoted as D1-601) with 61 stages (including a partial reboiler, numbering from top to bottom) has five feed streams (#21, #53, #54, #99 and #123) and one reflux stream (#127) feeding on the 1st stage. The draw-off stream #122 is designed for component PX in case it accumulates in the column. The bottom stream #109 is purified acetic acid and the mass fraction of HAc in the stream #109 is controlled at no less than 95%. Stream #125 is an uncondensed vapor gas outlet. Stream #126 is a removed water outlet. The entrainer NPA is recycled through an

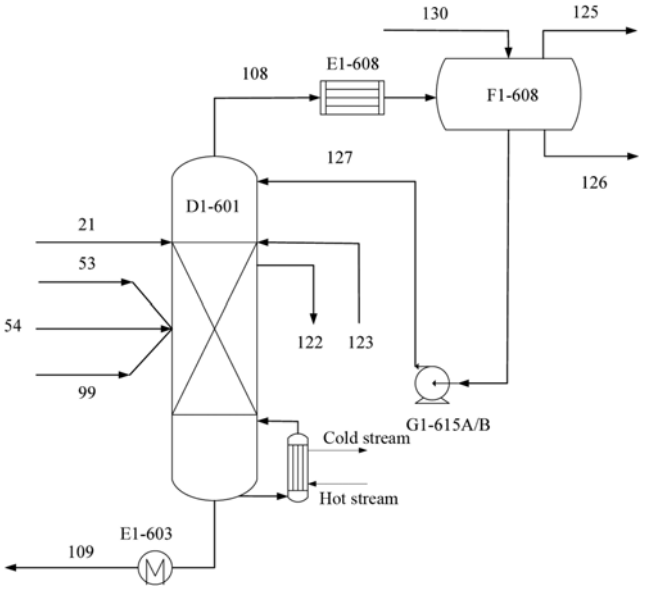

Fig. 1. Flow chart of solvent dehydrate distillation unit.

Table 1. Azeotropic analysis in the azeotropic distillation system

No.	T/°C	Azeotropic type	Mass fraction of components				
			HAc	H_2O	PX	MA	NPA
1	115.23	Homogeneous	0.6936		0.3064		
2	92.32	Heterogeneous		0.3439	0.6561		
3	56.64	Homogeneous		0.0233		0.9767	
4	83.05	Heterogeneous		0.1640			0.8360

Table 2. HAc-H_2O-entrainer three-phase mechanism model for SDDC

Equations /Figures	Vapor-liquid-liquid-equilibrium range	Vapor-liquid-equilibrium range
Figure	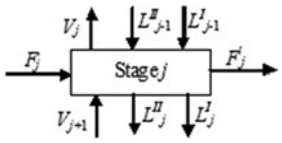	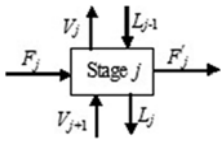
M	$V_{j+1}y_{j+1,i}+L^{I}_{j-1}x^{I}_{j-1,i}+L^{II}_{j-1}x^{II}_{j-1,i}+F_jx_{F,i}-V_jy_{j,i}-L^{I}_jx^{I}_{j,i}-L^{II}_jx^{II}_{j,i}-F'_jx_{j,i}=0$	$V_{j+1}y_{j+1,i}+L_{j-1}x_{j-1,i}+F_jx_{F,i}-V_jy_{j,i}-L_jx_{j,i}-F'_jx_{j,i}=0$
E	$P_j\phi_{j,i}y_{j,i}=f_i^{0L}x^{I}_{j,i}\gamma^{I}_{j,i}$ $P_j\phi_{j,i}y_{j,i}=f_i^{0L}x^{II}_{j,i}\gamma^{II}_{j,i}$ $x^{I}_{j,i}\gamma^{I}_{j,i}=x^{II}_{j,i}\gamma^{II}_{j,i}$	$P_j\phi_{j,i}y_{j,i}=f_i^{0L}x_{j,i}\gamma_{j,i}$
S	$\sum_{i=1}^{5}y_{j,i}-1=0,\ \sum_{i=1}^{5}x^{I}_{j,i}-1=0,\ \sum_{i=1}^{5}x^{II}_{j,i}-1=0$	$\sum_{i=1}^{5}y_{j,i}-1=0,\ \sum_{i=1}^{5}x_{j,i}-1=0$
T	$Eff^{M}_{j,i}=\frac{y_{j,i}-y_{j+1,i}}{K_{j,i}x_{j,i}-y_{j+1,i}}$	$Eff^{M}_{j,i}=\frac{y_{j,i}-y_{j+1,i}}{K_{j,i}x_{j,i}-y_{j+1,i}}$
H	$V_{j+1}H^{V}_{j+1}+L^{I}_{j-1}H^{I,L}_{j-1}+L^{II}_{j-1}H^{II,L}_{j-1}+F_jH^{F}_j-V_jH^{V}_j-L^{I}_jH^{I,L}_j-L^{II}_jH^{II,L}_j-F'_jH^{F'}_j=0$	$V_{j+1}H^{V}_{j+1}+L_{j-1}H^{L}_{j-1}+F_jH^{F}_j-V_jH^{V}_j-L_jH^{L}_j-F'_jH^{F'}_j=0$

organic reflux stream from the decanter. Stream #130 is used to make up for the loss of the entrainer.

2. Thermodynamic Equations

In the acetic acid azeotropic dehydration distillation system, there are five key components considered: acetic acid, water, NPA, PX and methyl acetate (MA); Table 1 shows the result of azeotropic analysis. The extended universal quasichemical (UNIQUAC) binary parameters for this azeotropic system were reported to predict the non-ideality in liquid phase well [14]. Thus, the UNIQUAC model was used to describe the activity coefficients of the liquid phases. Second virial coefficients of Hayden and O'Connell [15] were used to account for the vapor-phase association of acetic acid due to dimerization and trimerization.

3. METSH Equations

The mechanism model was built based upon a rigorous equilibrium stage model for solving the mass balance (M), phase equilibrium (E), tray efficiency equation (T), summation (S) and energy balance (H) equations. In the industrial SDDC, the equilibrium state can never be reached on each stage, so the actual separation character is described by using tray efficiency. Because of liquid phase split, the METSH equations should be divided into two parts as follows.

Tray efficiency is generally calculated as the Murphree efficiency, which is defined either in terms of liquid or vapor composition. Murphree efficiency is denoted as $Eff^{M}_{j,i}$ in Table 2, in which i represents one of the five key components and takes one value from [1-5], and j denotes the *j*th stage.

TRAY EFFICIENCY MODEL BASED ON BP NEURAL NETWORKS

1. Tray Efficiency Model Hypothesis

According to the feed positions, the industrial SDDC was divided into three sections as shown in Fig. 2. The streams are fed into both ends of each section, and there is no stream fed into the middle of each section. Thus, the vapor and liquid flow rates vary very little within each section, and tray efficiencies may not change drastically within each section. Thus, to simplify the model of the industrial SDDC, the hypothesis is that in each section Murphree efficiency of each component has linear relationship with stage numbers, and that Murphree efficiencies between two adjoining sections, i.e., $Eff^{M}_{1,i}$, $Eff^{M}_{21,i}$, $Eff^{M}_{46,i}$ and $Eff^{M}_{60,i}$, may change drastically due to the feeding streams. Murphree efficiency of component i on stage j can be calculated as follows.

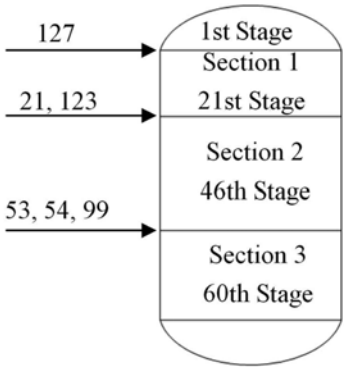

Fig. 2. Three sections of SDDC.

$$\begin{cases} Eff^{M}_{j,i} = Eff^{M}_{1,i} + \dfrac{Eff^{M}_{21,i} - Eff^{M}_{1,i}}{20} \times (j-1), & 1 \le j \le 21 \\ Eff^{M}_{j,i} = Eff^{M}_{21,i} + \dfrac{Eff^{M}_{46,i} - Eff^{M}_{21,i}}{25} \times (j-21), & 21 \le j \le 46 \\ Eff^{M}_{j,i} = Eff^{M}_{46,i} + \dfrac{Eff^{M}_{60,i} - Eff^{M}_{46,i}}{24} \times (j-46), & 46 \le j \le 60 \end{cases} \quad (1)$$

All tray efficiencies are determined for the industrial SDDC when the values of $Eff^{M}_{1,i}$, $Eff^{M}_{21,i}$, $Eff^{M}_{46,i}$ and $Eff^{M}_{60,i}$ are obtained.

2. Collect the Sample Data for Tray Efficiency Model

To develop the tray efficiency model via neural network, the sample data, which include the operation conditions of the industrial SDDC and the corresponding tray efficiencies, i.e., $Eff^{M}_{1,i}$, $Eff^{M}_{21,i}$, $Eff^{M}_{46,i}$ and $Eff^{M}_{60,i}$, are needed. Because the tray efficiencies are not direct measurement variables, the following procedure is employed to determine the tray efficiencies under various operation conditions: (1) Initialize $Eff^{M}_{1,i}$, $Eff^{M}_{21,i}$, $Eff^{M}_{46,i}$ and $Eff^{M}_{60,i}$ for a operation state; (2) Use the operation conditions to run the mechanism SDDC model with $Eff^{M}_{1,i}$, $Eff^{M}_{21,i}$, $Eff^{M}_{46,i}$ and $Eff^{M}_{60,i}$, which is developed via Aspen Plus® [16]; (3) Calculate the deviation between the simulation results and the measurement data. If the deviation reaches a satisfactory small level, the optimal tray efficiencies are obtained. Otherwise, adjust the tray efficiencies and go back step (2).

The main object of the procedure is to minimize the deviation between simulation results and measurement data via adjusting the tray efficiencies, i.e., $Eff^{M}_{1,i}$, $Eff^{M}_{21,i}$, $Eff^{M}_{46,i}$ and $Eff^{M}_{60,i}$ by trial and error. The tray efficiencies, which correspond to the minimum deviation, are the optimal tray efficiencies relative to the corresponding operation conditions. Namely, the optimal tray efficiencies and the corresponding operation conditions are a pair of sample data.

The industrial SDDC, which is one unit of continuous processing plants, is running in an uninterrupted, continuous way. After the start-up phase of the plant, it is operated in more or less constant and hopefully optimal state, so the industrial SDDC model focuses on the description of the steady-state. Because the quality of the sample data almost determines the performance of the neural network of Murphree efficiency, as many as possible typical steady-state operation data have been collected in the long-term operation of the plant. To determine the accuracy of the tray efficiency model, the collected sample data must be different steady-state data and it is the best if they are distributed uniformly within whole domain of operation conditions. Finally, 12 representative samples data of steady states were collected from a large number process data of the industrial SDDC. They include the operation conditions from the lowest flow of the main input feed to its maximum flow to guarantee the performance of the neural network model. The values of important variables are listed in Table 6. Twelve different mechanism models with their respective optimal tray efficiencies are developed

Table 3. Murphree efficiencies on the first stage of each section

Stage	HAc	NPA	PX	H_2O	MA
1	0.4	0.001	0.32	1	1
21	0.9	*	0.6	1	1
46	0.6	0.5	0.4	1	1
60	0.4	0.5	0.5	1	1

Note: The * value varies according to operation states

based on 12 representative sample data, and the simulation results are shown in Table 7. Tables 3 and 7 show the obtained optimal tray efficiencies. It can be shown that all tray efficiencies are constant except for Murphree efficiency of NPA on the #21 stage, i.e., $Eff_{21,2}^{M}$, for 12 representative samples data of steady states.

3. Determine the Input and Output Variables for Tray Efficiency Model

Figs. 3 and 4 show the liquid and vapor composition profiles of the industrial SDDC under one representative operation state. It can be seen that the fractionation is primarily between HAc and NPA, the composition of NPA around the #21 stage changes drastically, and NPA dies out quite rapidly in both the liquid and vapor streams beneath the #21 stage. Meanwhile, the results shown in Tables 3 and 8 demonstrate that the Murphree efficiency of NPA on the #21 stage is sensitive to the change of the operation conditions, and that the other tray efficiencies are insensitive and all constant. Thus, the Murphree efficiency of NPA on the #21 stage is regarded as only one output variable of the neural network model.

The input variables of the neural network should be measured easily and closely related to the fractionation of the industrial SDDC. Figs. 3 and 4 show that the main change of the composition content happens within 10th-57th stages. Because tray temperature profile represents the fractionation performance of the industrial SDDC, two available tray temperatures, the 10th tray temperature and the 57th tray temperature, which are two available temperatures except for bottom and top temperatures, are selected as two input variables. According to the distillation mechanism, the flowrate of stream #21 and the pressure drop of the overall column, which equals to the bottom pressure minus the top pressure, are selected as the other two input variables because their data were available at hand and they

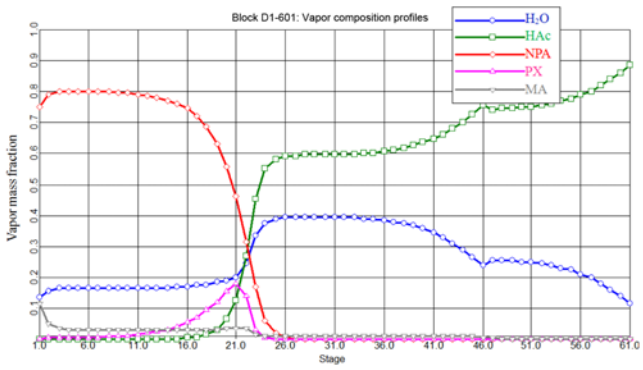

Fig. 3. Vapor composition profiles.

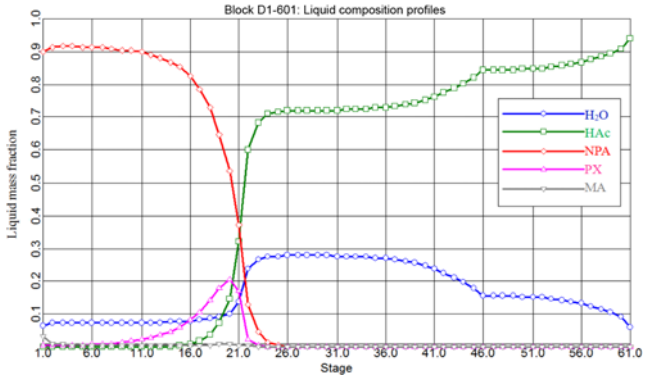

Fig. 4. Liquid composition profiles.

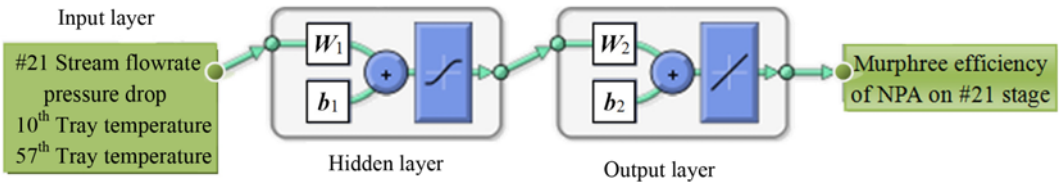

Fig. 5. The structures of two neural networks with one or two hidden neurons.

Table 4. Performances of two neural networks

No.	Input				Output		
	Flowrate of stream 21 (t/hr)	Pressure drop (kPa)	T10 °C	T57 °C	Real value	Output with one neuron	Output with two neurons
1	50.25	27.03	85.8	112.7	0.3	0.2946	0.3048
2	52.67	27.9	85.4	113.0	0.4	0.4149	0.3888
3	53.41	28.09	85.2	112.7	0.45	0.4513	0.4487
4	56.33	28.29	85.4	112.9	0.6	0.5541	0.5429
5	57.25	27.6	86.6	112.8	0.5	0.5261	0.4822
6	62.75	31.67	85.7	113.5	0.8	0.8352	0.7432
7	64.39	30.16	85.5	112.6	0.78	0.8151	0.7972
8	67.93	30.86	85.7	112.9	0.9	0.8522	0.8787
9	69.92	31.2	85.6	113.0	0.9	0.863	0.8885
10	75.36	34.39	86.0	113.4	0.9	0.8804	0.8815
11	79.68	35.3	86.3	115.0	0.9	0.8818	0.8914
12	82.48	35.42	86.0	114.0	0.82	0.8821	0.8821

have the main effect on tray efficiency. Thus, four input variables are chosen for the neural network.

4. Neural Networks Model of Tray Efficiency

The number of hidden neurons plays an important role in the performance of neural networks [17]. Considering that there are only 12 representative sample data and that there is an over-parameterization on condition that the number of hidden neurons is equal to or more than 3, two neural networks with one and two hidden neuron(s) are employed to develop the Murphree efficiency model of NPA on the #21 stage with four input variables. The structures of two neural networks are shown in Fig. 5. The activation function of hidden layer is a hyperbolic tangent sigmoid transfer function ('tansig' function in Matlab® [18]), and the activation function of output layer is a linear transfer function ('purelin' function in Matlab® [18]). The performance criterion for neural network evaluation

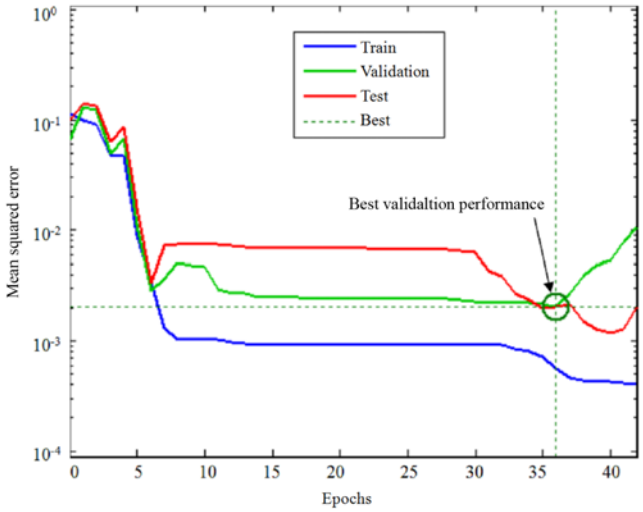

Fig. 6. The performance criterion curves of neural network with epoch.

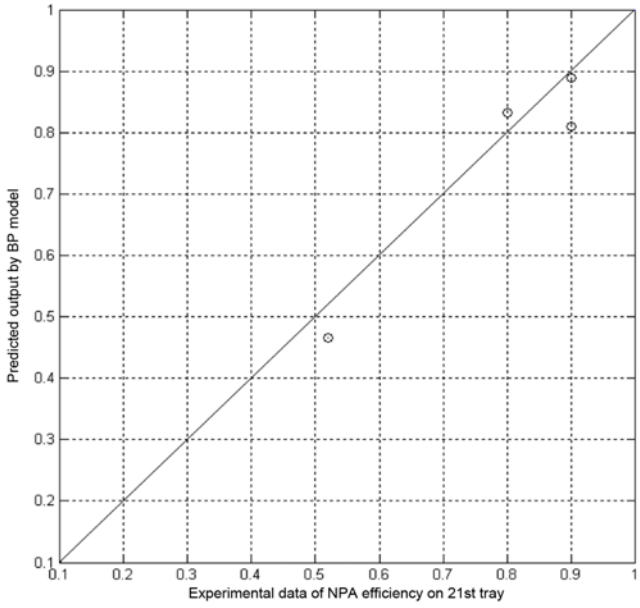

Fig. 7. Prediction performance of NN with one neuron.

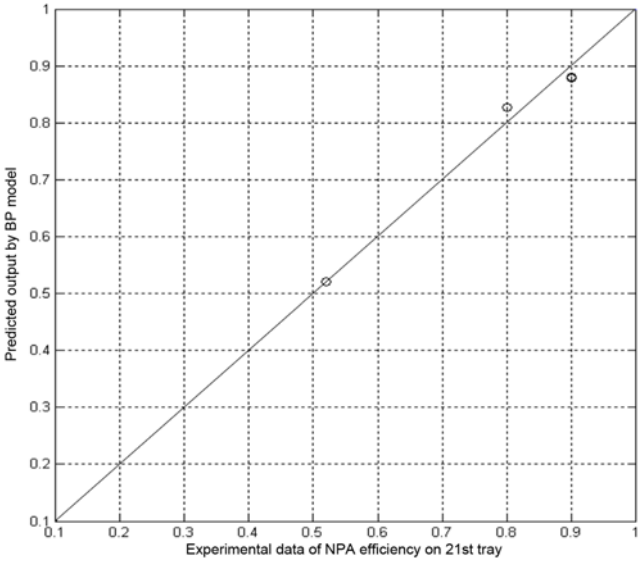

Fig. 8. Prediction performance of NN with two neurons.

is mean squared error. Levenberg-Marquardt back propagation method [19] was employed to train the neural network.

The results of two neural networks shown in Table 4 demonstrate that the performance of the neural network with two hidden neurons is a little better than the neural network with one hidden neuron. Fig. 6 shows the training process of neural network with two hidden neurons. To validate two neural network models, another four operation states and the corresponding Murphree efficiencies of NPA on the #21 stage, which are not used for train and cross validation, are employed. The predicting performances of two neural networks are shown in Figs. 7 and 8. The results also demonstrate that the performance of the neural network with two hidden neurons is a little better than the neural network with one hidden neuron.

Thus, the neural network model with two hidden neurons is chosen as the model of Murphree efficiencies of NPA on the #21 stage.

HYBRID MODEL OF INDUSTRIAL SOLVENT DEHYDRATION DISTILLATION COLUMN

1. Procedure of Hybrid Model

After the neural network model of Murphree efficiencies of NPA on the #21 stage is developed in Matlab®, the neural network model is translated via Fortran language and embedded into the Aspen plus® distillation model as a calculator block of the Aspen plus®. Meanwhile, Eq. (1) for calculating Murphree efficiency of component i on stage j is embedded into the Aspen plus® distillation model as another calculator block. Define the sequence of two calculator blocks and distillation column in the Aspen plus®, and the procedure of hybrid model for the industrial SDDC is as follows.

Step1: Operation conditions of the industrial SDDC are collected.

Step2: The neural network model with two hidden neurons is used to calculate Murphree efficiencies of NPA on the #21 stage, i.e. $\mathrm{Eff}^{M}_{21,2}$.

Step3: $\mathrm{Eff}^{M}_{21,i}$ (i=1, 3, 4), $\mathrm{Eff}^{M}_{1,i}$, $\mathrm{Eff}^{M}_{46,i}$ and $\mathrm{Eff}^{M}_{60,i}$ obtained from Table 4 are employed with $\mathrm{Eff}^{M}_{21,2}$ to calculate tray efficiencies of each stage and each component according to the Eqs. (1).

Step4: The mechanism model with the estimated tray efficiencies

Table 5. Performance comparison between the hybrid model and three mechanism models

#21 ton/hr	Murphree efficiency of NPA on 21st stage				Operation condition	Field data	Simulation result			
	Hybrid model	Model1	Model2	Model3			Hybrid model	Model1	Model2	Model3
55.97	0.51	0.30	0.78	0.82	10th Stage temperature (°C)	85.5	85.2	86.0	**	**
					57th Stage temperature (°C)	112.2	112.7	112.7		
					Top pressure (kPa)	108.7	108.7	108.7		
					Bottom pressure (kPa)	127.5	127.5	127.5		
					Top distillate (ton/hr)	28.03	28.03	28.03		
65.29	0.79	0.30	0.78	0.82	10th Stage temperature (°C)	85.8	85.5	**	85.5	85.6
					57th Stage temperature (°C)	112.3	112.6		112.7	112.6
					Top pressure (kPa)	109.5	109.5		109.5	109.5
					Bottom pressure (kPa)	129.5	129.5		129.5	129.5
					Top distillate (ton/hr)	30.30	30.30		30.30	30.30
72.69	0.89	0.30	0.78	0.82	10th Stage temperature (°C)	85.8	85.6	**	85.9	85.4
					57th Stage temperature (°C)	112.7	112.5		113.4	113.5
					Top pressure (kPa)	110.6	110.6		110.6	110.6
					Bottom pressure (kPa)	131.4	131.4		131.4	131.4
					Top distillate (ton/hr)	34.37	34.37		34.37	34.37
77.00	0.86	0.30	0.78	0.82	10th Stage temperature (°C)	86.1	86.2	**	86.3	86.2
					57th Stage temperature (°C)	113.8	113.7		113.2	113.3
					Top pressure (kPa)	111.4	111.4		111.4	111.4
					Bottom pressure (kPa)	131.3	131.3		131.3	131.3
					Top distillate (ton/hr)	34.53	34.53		34.53	34.53

Note: F21 means flowrate of stream 21; Model1 is the 1st model in Table 7. Model2 is the 7th model in Table 7. Model3 is the 12th model in Table 7
** Means that the rigorous mechanism model is not convergent

is employed to simulate the industrial SDDC with the operation conditions.

2. Hybrid Model Performance Analysis

Four new industrial operation states are collected for testing the performance of the hybrid model and the other three mechanism models, which are developed in Aspen plus® based on the operation state 1, 7 and 12 in Table 6, respectively, and whose efficiencies of NPA on 21st stage are constant: 0.3, 0.78 and 0.82. The simulation results are shown in Table 5. The results in Table 5 show that the hybrid model has the most robustness among the four models, and when the industrial operation states are far from the operation state whose data is employed to develop mechanism model, the corresponding mechanism model may be un-convergent.

3. Operation Analysis Using the Hybrid Model

In the industrial column, the column bottom product is kept at 95.0% mass HAc, which is re-cycled back to the oxidation reactor as the solvent. The HAc purity can be controlled by varying the reboiler duty. On condition that the operation conditions except for the bottom flow rate are fixed, the bottom flow rate has an obvious impact on the bottom product compositions, i.e., HAc, NPA and H_2O mass fraction of bottom flow represented by x_{HAc}, x_{NPA} and x_{H_2O}, respectively. It can be seen from Fig. 9 that, when the bottom flow rate is bigger than some value, i.e., 132 (tonne/hr), the entrainer loss through bottom product begins to increase, which should be avoided in real-life operating for economic reasons. Furthermore, the bottom flow rate determines the purity level of HAc. As shown in Fig. 10, when the bottom flow rate is set at some value, the concentration of HAc can only reach a certain level, no matter how large the reflux

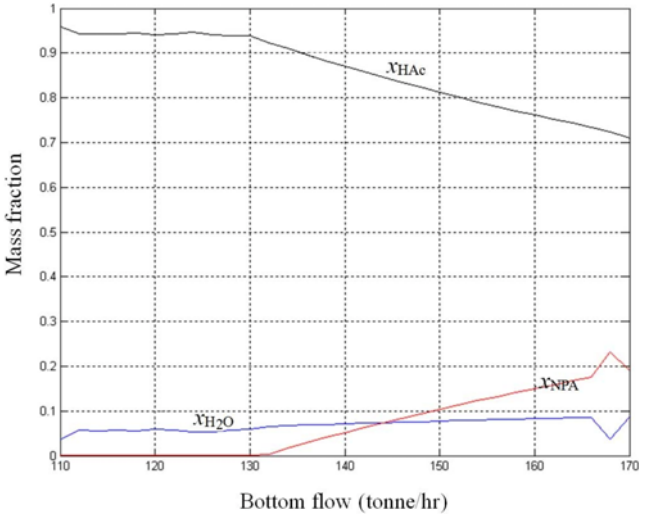

Fig. 9. Mass fraction curves of bottom composition with bottom flow rate.

rate is.

In the decanter, two liquid phases form. One rich in NPA is called the organic phase, and the other rich in water is called the aqueous phase. All the organic phase and portion of the aqueous phase are refluxed back to the column. The reflux flow rate #127 relates to the energy consumption of the distillation system, and influences the column product compositions. It can be seen from Fig. 11 that when the reflux flow rate is large enough, the product compositions

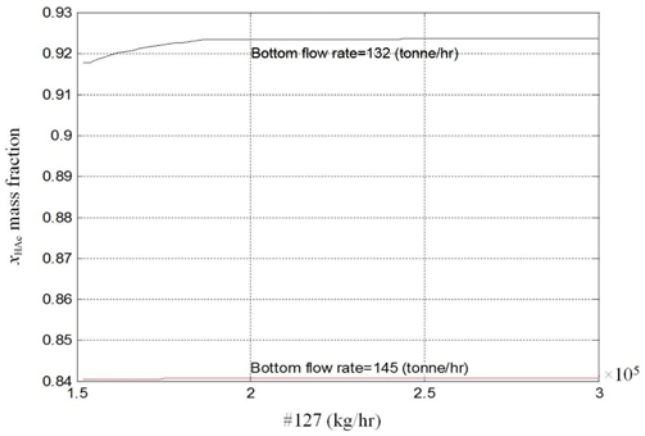

Fig. 10. HAc mass fraction of bottom product with reflux rate and bottom flow rate.

stay almost unchanged. Thus, the up limit of the #127 can be determined according to the turning point of HAc mass fraction of bottom flow (x_{HAC}), i.e., 215 (ton/h), to avoid energy waste. But when the reflux flow rate is smaller than certain value, i.e., 175 (ton/h), the water composition (x_{H_2O}) in the aqueous outlet decreases drastically and the HAc composition in the bottom is diluted because there is not enough NPA to carry the water out from the top of the column. Thus, the turning point of x_{H_2O} in Fig. 11 can be treated as the low limit of reflux flow rate. At the same time, it can be seen from Fig. 12 that the water composition in the aqueous outlet varies with NPA makeup flow rate. The reason is that within the heterogeneous region,

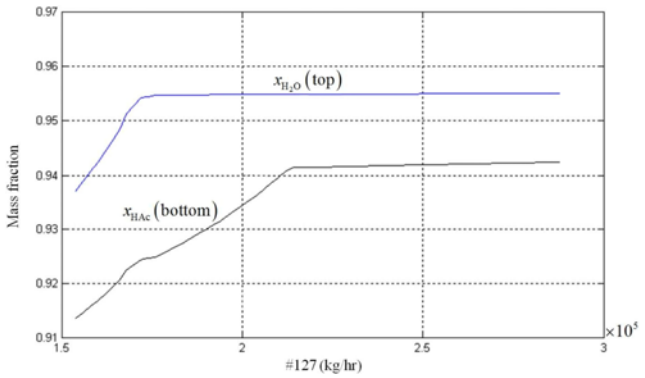

Fig. 11. Bottom and top product compositions varying with reflux flow rate.

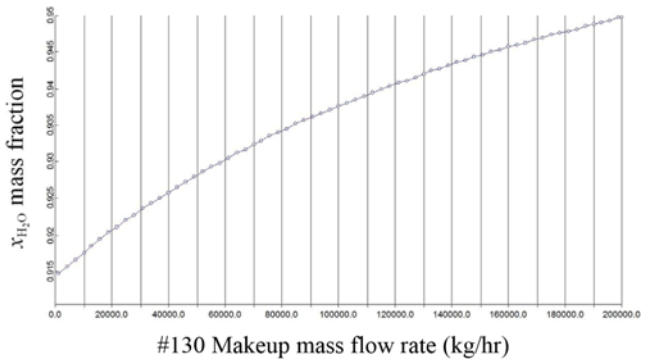

Fig. 12. H_2O compositions varying with #130 makeup flow rate.

more NPA the mixing liquid contains, higher water purity will be reached at the aqueous phase. The aqueous phase contains a very little entrainer and the aqueous phase stream will be drawn out of the system. The loss of the entrainer happens.

CONCLUSIONS

The hybrid model of the industrial SDDC demonstrates good predicting and robust performance. The neural network tray efficiency model can provide the proper tray efficiencies for each component at each stage according to the industrial operation conditions. Compared with the measurement data, the distillation mechanism model with the obtained tray efficiencies predicts the industrial SDDC fairly well. Compared with the traditional distillation mechanism model with constant tray efficiencies, the hybrid model has better predicting accuracy and robustness. Based on the hybrid model, the effect of key operation conditions is analyzed and some useful guiding rules are obtained. Because the predicting performance of the neural network depends on the quality and range of the sample data, the performance of the hybrid model also depends on the quality and range of the sample data.

ACKNOWLEDGEMENTS

The authors gratefully acknowledge the support from the following foundations: National Natural Science Foundation of China (21176073), Doctoral Fund of Ministry of Education of China (20090074110005), Program for New Century Excellent Talents in University (NCET-09-0346), "Shu Guang" project (09SG29), 973 project (2012CB721006) and the Fundamental Research Funds for the Central Universities.

NOMENCLATURE

$Eff_{j,i}^{M}$: murphree efficiency of component i at stage j
$x_{j,i}$: mole fraction of component i in the liquid phase at stage j
$y_{j,i}$: mole fraction of component i in the vapor phase at stage j
$K_{j,i}$: equilibrium $K_{j,i}$ value of component i in the liquid phase at stage j
H_j^L : molar enthalpy of liquid at stage j
H_j^V : molar enthalpy of vapor at stage j
V_j : vapor flow rate at stage j
L_j : liquid flow rate at stage j
P_j : pressure at stage j
$\phi_{i,i}$: fugacity coefficient of component i at stage j
$\gamma_{i,i}$: activity coefficient of component i at stage j
f_i^0 : fugacity of component i at normal state
F_j' : draw-off side stream flow rate at stage j
F_j : side feed stream flow rate at stage j
x_{HAc} : HAc mass fraction of flow
x_{NPA} : NPA mass fraction of flow
x_{H_2O} : H_2O mass fraction of flow
Note: I stands for 1st liquid; II stands for 2nd liquid

REFERENCES

1. J. Y. Jang, H. J. Kim and K. Wu, US Patent, 20,030,150,706 (2003).

2. M. M. Lee, D. J. Kwon, D. W. Lee and A. J. Lee, US Patent, 20,070,027,340 (2007).
3. D. F. Othmer, *Chem. Metall. Eng.*, **40**, 91 (1941).
4. I. L. Chien, K. L. Zeng, H. Y. Chao and J. H. Liu, *Chem. Eng. Sci.*, **59**, 4547 (2004).
5. S. Widagdo and W. D. Seider, *AIChE J.*, **42**, 96 (1996).
6. K. Hornik, M. Stinchombe and H. White, *Neural Networks*, **2**, 359 (1989).
7. E. Russell and Y. H. Shi, *Computational intelligence*, Morgan Kaufman Publication, Massachusetts (2007).
8. J. J. Hopfield, *P Natl. Acad. Sci. USA*, **79**, 2554 (1982).
9. G. Cybenco, *Math. Control. Signal.*, **2**, 303 (1989).
10. F. Girosi and T. Poggio, *Biol. Cybern.*, **63**, 169 (1990).
11. D. E. Rumelhart, G. E. Hinton and R. J. Williams, *Nature (London)*, **323**, 533 (1986).
12. T. P. Vogl, J. K. Mangis, A. K. Rigler, W. T. Zink and D. L. Alkon, *Biol. Cybern.*, **59**, 256 (1988).
13. L. E. Scales, *Introduction to non-linear optimization*, Springer-Verlag, New York (1985).
14. D. S. Abrams and J. M. Prausnitz, *AIChE J.*, **21**, 116 (1975).
15. J. G. Hayden and J. P. O'Connell, *Ind. Eng. Chem., Process Des. Dev.*, **14**, 209 (1975).
16. Aspen Technology, Inc., *Aspen Plus*®, http://www.aspentech.com/core/aspen-plus.aspx.
17. X. F. Yan. *Chemometr. Intell. Lab. Syst.*, **103**, 152 (2010).
18. MathWorks, Inc., *Matlab*®, http://www.mathworks.cn/products/matlab/.
19. K. Levenberg, *Q. Appl. Math.*, **2**, 164 (1944).

SUPPLEMENTARY

Table 6. SDDC feed streams data of 12 representative samples

Sample no.	Stream no.	Temperature °C	Pressure kPa	Flowrate ton/hr	Sample no.	Stream no.	Temperature °C	Pressure kPa	Flowrate ton/hr
1	21	80	1510	50.25	7	21	80	1510	64.39
	53	122	1170	16.93		53	122	1170	21.69
	54	161.7	430	14.25		54	161.7	430	18.26
	99	121	140	27.01		99	121	140	34.61
	123	94.6	130	2.13		123	94.6	130	2.73
	127	76.3	300	158.13		127	76.3	300	189.94
2	21	80	1510	52.67	8	21	80	1510	67.93
	53	122	1170	17.75		53	122	1170	22.89
	54	161.7	430	14.94		54	161.7	430	19.27
	99	121	140	28.31		99	121	140	36.51
	123	94.6	130	2.25		123	94.6	130	2.82
	127	76.5	300	151.26		127	76.4	300	202.80
3	21	80	1510	53.41	9	21	80	1510	69.92
	53	122	1170	18.00		53	122	1170	23.56
	54	161.7	430	15.15		54	161.7	430	19.83
	99	121	140	28.71		99	121	140	37.58
	123	94.6	130	2.26		123	94.6	130	2.97
	127	76.4	300	169.08		127	76.1	300	202.04
4	21	80	1510	56.33	10	21	80	1510	75.36
	53	122	1170	18.98		53	122	1170	25.39
	54	161.7	430	15.98		54	161.7	430	21.38
	99	121	140	30.28		99	121	140	40.51
	123	94.6	130	2.39		123	94.6	130	3.20
	127	76.4	300	179.76		127	76.0	300	223.38
5	21	80	1510	57.25	11	21	80	1510	79.68
	53	122	1170	19.29		53	122	1170	26.85
	54	161.7	430	16.24		54	161.7	430	22.60
	99	121	140	30.77		99	121	140	42.83
	123	94.6	130	2.43		123	94.6	130	3.38
	127	76.2	300	160.92		127	75.8	300	227.92
6	21	80	1510	62.75	12	21	80	1510	82.48
	53	122	1170	21.14		53	122	1170	27.79
	54	161.7	430	17.80		54	161.7	430	23.40
	99	121	140	33.73		99	121	140	44.34

Table 6. Continued

Sample no.	Stream no.	Temperature °C	Pressure kPa	Flowrate ton/hr	Sample no.	Stream no.	Temperature °C	Pressure kPa	Flowrate ton/hr
	123	94.6	130	2.66		123	94.6	130	3.50
	127	76.4	300	185.81		127	76.0	300	236.26

Table 7. Measurement values and simulation values of SDDC

Sample no.	Efficiency*	Variable	Measurement value	Simulation value	Relative error (%)
1	0.30	10th Tray temperature (°C)	85.7	85.8	0.12
		57th Tray temperature (°C)	112.7	112.0	0.62
		Top Pressure (kPa)	107.3	107.3	0
		Bottom Pressure (kPa)	125.7	125.7	0
		Top distillate rate (ton/hr)	27.0	27.0	0
2	0.40	10th Tray temperature (°C)	86.0	86.9	1.0
		57th Tray temperature (°C)	112.9	113.1	0.18
		Top Pressure (kPa)	107.1	107.1	0
		Bottom Pressure (kPa)	125.3	125.3	0
		Top distillate rate (ton/hr)	26.6	26.6	0
3	0.45	10th Tray temperature (°C)	85.2	85.2	0.12
		57th Tray temperature (°C)	113.8	112.7	0.96
		Top Pressure (kPa)	106.8	106.8	0
		Bottom Pressure (kPa)	125.3	125.3	0
		Top distillate rate (ton/hr)	28.1	28.1	0
4	0.60	10th Tray temperature (°C)	85.3	85.3	0.00
		57th Tray temperature (°C)	111.2	112.1	0.81
		Top Pressure (kPa)	108.4	108.4	0
		Bottom Pressure (kPa)	127	127	0
		Top distillate rate (ton/hr)	28.2	28.2	0.35
5	0.50	10th Tray temperature (°C)	86.7	85.5	1.38
		57th Tray temperature (°C)	127.0	112.6	0
		Top Pressure (kPa)	108.3	108.3	0
		Bottom Pressure (kPa)	126.7	126.7	0
		Top distillate rate (ton/hr)	27.7	27.7	0
6	0.80	10th Tray temperature (°C)	86.3	85.7	0.7
		57th Tray temperature (°C)	113.7	112.9	0.7
		Top Pressure (kPa)	110.2	110.2	0
		Bottom Pressure (kPa)	129.7	129.7	0
		Top distillate rate (ton/hr)	31.5	31.5	0
7	0.78	10th Tray temperature (°C)	85.7	85.5	0.23
		57th Tray temperature (°C)	112.2	112.6	0.36
		Top Pressure (kPa)	109.2	109.2	0
		Bottom Pressure (kPa)	128.9	128.9	0
		Top distillate rate (ton/hr)	30.2	30.2	0
8	0.90	10th Tray temperature (°C)	86.0	85.7	0.35
		57th Tray temperature (°C)	112.9	112.8	0.09
		Top Pressure (kPa)	110	110	0
		Bottom Pressure (kPa)	130.2	130.2	0
		Top distillate rate (ton/hr)	30.8	30.8	0
9	0.90	10th Tray temperature (°C)	85.7	85.6	0.12
		57th Tray temperature (°C)	113.3	113.4	0.09
		Top Pressure (kPa)	109.9	109.9	0
		Bottom Pressure (kPa)	130.3	130.3	0
		Top distillate rate (ton/hr)	31.2	31.2	0

Table 7. Continued

Sample no.	Efficiency*	Variable	Measurement value	Simulation value	Relative error (%)
10	0.90	10^{th} Tray temperature (°C)	86.2	86.0	0.23
		57^{th} Tray temperature (°C)	113.4	113.4	0
		Top Pressure (kPa)	111.1	111.1	0
		Bottom Pressure (kPa)	132.1	132.1	0
		Top distillate rate (ton/hr)	34.4	34.4	0
11	0.90	10^{th} Tray temperature (°C)	86.6	86.3	0.35
		57^{th} Tray temperature (°C)	115.3	114.0	1.13
		Top Pressure (kPa)	112	112	0
		Bottom Pressure (kPa)	132.9	132.9	0
		Top distillate rate (ton/hr)	35.3	35.3	0
12	0.82	10^{th} Tray temperature (°C)	86.4	86.0	0.46
		57^{th} Tray temperature (°C)	114.2	113.2	0.88
		Top Pressure (kPa)	110.4	110.4	0
		Bottom Pressure (kPa)	131.9	131.9	0
		Top distillate rate (ton/hr)	35.3	35.3	0

Note: Efficiency means the value of NPA Murphree efficiency on #21st stage